A Two-Port Microstrip Antenna With High Isolation for Wi-Fi 6 and Wi-Fi 6E Applications

Weiquan Zhang, Yue Li, *Senior Member, IEEE*, Kunpeng Wei, *Senior Member, IEEE*, and Zhijun Zhang, *Fellow, IEEE*

***Abstract*— In this article, a two-port microstrip antenna (MSA) with high isolation is presented for simultaneously supporting wireless fidelity 6 (Wi-Fi 6) and wireless fidelity 6E (Wi-Fi 6E) applications. Due to the narrow guard band between Wi-Fi 6 (5.15–5.83 GHz) and Wi-Fi 6E (5.92–7.125 GHz), the mutual coupling near common edge frequencies cannot be sufficiently suppressed by existing filters. To mitigate the mutual coupling over the guard band of a symmetrical two-port MSA, the common-mode (CM)/differential-mode (DM) cancellation theory was utilized. Then, the operating frequencies of two ports were tuned to Wi-Fi 6 and Wi-Fi 6E bands, without deteriorating the original decoupling performance. Finally, two filters were loaded to realize high isolation over the whole working bandwidth. For the demonstration, a prototype was fabricated and measured. The measured results show that the proposed two-port MSA achieves the impedance bandwidth of 5.49–5.9 and 5.89–7.14 GHz and the isolation over 20 dB across the whole band. The results indicate that the proposed antenna is a promising candidate for Wi-Fi 6 and Wi-Fi 6E applications.**

***Index Terms*— Adjacent frequency band, microstrip antenna (MSA), mutual coupling reduction, Wi-Fi.**

I. Introduction

With the rapid development of modern communication system, the existing scarce frequencies are getting crowded. Therefore, different communication systems are frequently integrated together to support several communication standards. Mutual coupling is unavoidable when two antennas are closely located with the same or close operating bands, such as wireless fidelity 6 (Wi-Fi 6) and wireless fidelity 6E (Wi-Fi 6E) bands. Interference caused by mutual coupling in wireless networks has become an important issue to achieve higher network capacity [1]. There are many works concerning antennas operating in the same frequency bands [2]–[8]. However, it is common sense that communication systems with different operating frequencies are packed together to occupy small space [9]. The mutual coupling is neglectable for two closely located antennas with markedly different working bands [9]–[11]. Predictably, interference has inevitably occurred for two antennas with adjacent/contiguous frequency bands since the guard band is limited/nonexistent. As shown in Fig. 1, when a compact communication system simultaneously supports Wi-Fi 6 and Wi-Fi 6E standards, interference becomes a very serious problem due to the narrow guard band (0.09 GHz).

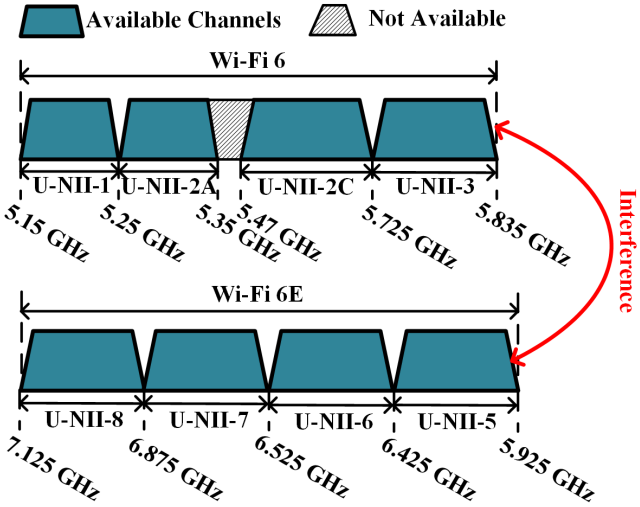

Fig. 1. Frequency bands for Wi-Fi 6 and Wi-Fi 6E.

To mitigate the mutual coupling of antennas resonating at close/contiguous frequencies, significant efforts from industry and academic communities have been devoted. To decrease mutual coupling, one common approach is to apply filtering structures around the antenna elements [12]–[17]. By loading two open-loop resonators at both sides of the feed-line, two microstrip antennas (MSAs) were proposed in [12] with adjacent operating bands and high isolation. In [13], band-notched slot antennas were proposed with radiation-suppression characteristics at the notch frequencies for high isolation. High-pass substrate integrated waveguide and low-pass spoof surface plasmon polariton were designed and applied in the feeding network for realizing broadband decoupling [15]. Decoupling networks were also studied to mitigate coupling between two antennas resonating in adjacent/contiguous frequency bands [18]–[22]. A coupled-resonator decoupling network and its chip realization based on the low-temperature cofired ceramic technique were presented in [18] and [19] but with complicated structures and

Manuscript received 29 October 2021; revised 24 December 2021; accepted 5 January 2022. Date of publication 28 January 2022; date of current version 26 July 2022. This work was supported in part by the National Natural Science Foundation of China under Contract 61971254. *(Corresponding author: Zhijun Zhang.)*

Weiquan Zhang, Yue Li, and Zhijun Zhang are with the Department of Electronic Engineering and the Beijing National Research Center for Information Science and Technology, Tsinghua University, Beijing 100084, China (e-mail: zjzh@tsinghua.edu.cn).

Kunpeng Wei is with Honor Device Company Ltd., Beijing 100095, China.

Color versions of one or more figures in this article are available at https://doi.org/10.1109/TAP.2022.3145439.

Digital Object Identifier 10.1109/TAP.2022.3145439

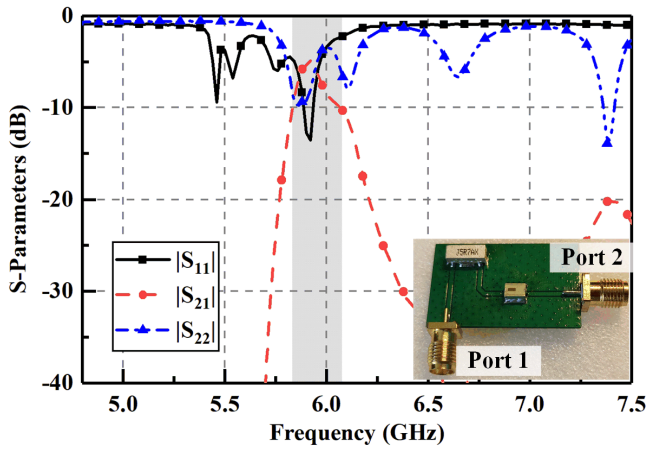

Fig. 2. Measured *S*-parameters for the cascaded filters and the fabricated protype.

optimization. In [20], a cascaded power dividing decoupling network was proposed to decrease the mutual coupling of two antennas resonating in close or even contiguous frequency bands. The orthogonal modes of antenna systems were excited by decoupling and matching networks in [21] and [22]. High port-to-port isolation was guaranteed by the intrinsic orthogonality of the modes but with distinct radiation patterns for each mode. To effectively reduce the mutual coupling, a high-isolation diplexer was designed in [23].

Filters are frequently applied in RF front ends to mitigate mutual coupling in industry. However, filters usually cannot effectively depress the mutual coupling for two antennas operating at adjacent/contiguous frequency bands since the mutual coupling near common edge frequencies cannot be sufficiently suppressed. To prove this point, a test was carried out. Two ceramic bandpass filters were selected. The operating passband of Johanson 5697CR45A0360 is 5.49–5.85 GHz covering the U-NII-2C and U-NII-3 bands of Wi-Fi 6. Also, the passband of Johanson 6530BP44A1190 is 5.925–7.125 GHz covering the whole Wi-Fi 6E bands. These two devices were cascaded and measured. As shown in Fig. 2, the measured mutual coupling of the cascaded filters is worse than −10 dB from 5.84 to 6.05 GHz with a maximum value of 4.9 dB at 5.92 GHz. Therefore, for two antennas with adjacent/contiguous frequency bands, it is still a challenge to achieve a broadband isolation by using only filters.

In this article, a two-port MSA with broadband decoupling is realized based on the common-mode (CM)/differential-mode (DM) cancellation theory and filters. By using the CM/DM cancellation theory, the isolation between the two ports of a symmetrical MSA was significantly enhanced at 6 GHz. Then, it was proven that the operating frequency of each port can be independently adjusted without destroying the original isolation performance. Hence, the working frequencies of the two ports can be independently tuned. Finally, broadband decoupling is achieved by adding the two filters.

The remainder of this article is organized as follows: In Section II, the working mechanism is presented and discussed. To verify the design scheme, the evolution process of a two-port MSA is given in detail. In Section III, the simulated and measured performances of the proposed antenna are demonstrated and analyzed. Finally, Section IV summarizes our work.

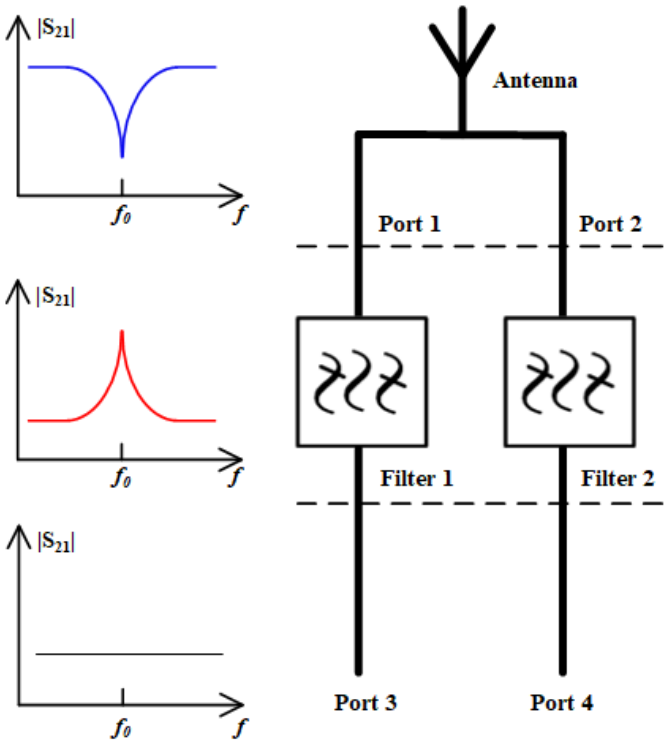

Fig. 3. Schematic of the broadband decoupling method.

II. Antenna Design

To achieve broadband mutual coupling reduction for antennas with adjacent/continuous operating bands, the CM/DM cancellation theory and filters are applied in this article. Fig. 3 shows the sketch diagram of a two-port antenna system. The two ports are operating at close/continuous bands and f_0 is the center frequency of the guard band. To compensate for the filtering performance of filters near f_0, a two-port antenna with high isolation at f_0 is desirable. As shown in Fig. 3, by combining the decoupling performance between the two ports and the filters, the mutual coupling can be effectively reduced across the whole bandwidth. The mutual coupling at f_0 can be mitigated based on the CM/DM cancellation theory [24], [25].

A. Port Decoupling

MSAs have been widely used in Wi-Fi applications. A two-port MSA is taken as an example here to describe the implementation of the decoupling process. Fig. 4 shows the sketch diagram of a two-port MSA I, which consists of one metal sheet, one FR4 substrate with the relative permittivity $\varepsilon_r = 4.4$ and the loss tangent of 0.02, and two feeding probes. Lumped ports were applied to feed the microstrip lines. The top layer of the substrate is used as the ground. Table I shows the detailed dimensions of MSA I. For the antenna, even-symmetrical property along the *xz* plane and the *yz* plane is observable. The antenna was simulated by the HFSS [26].

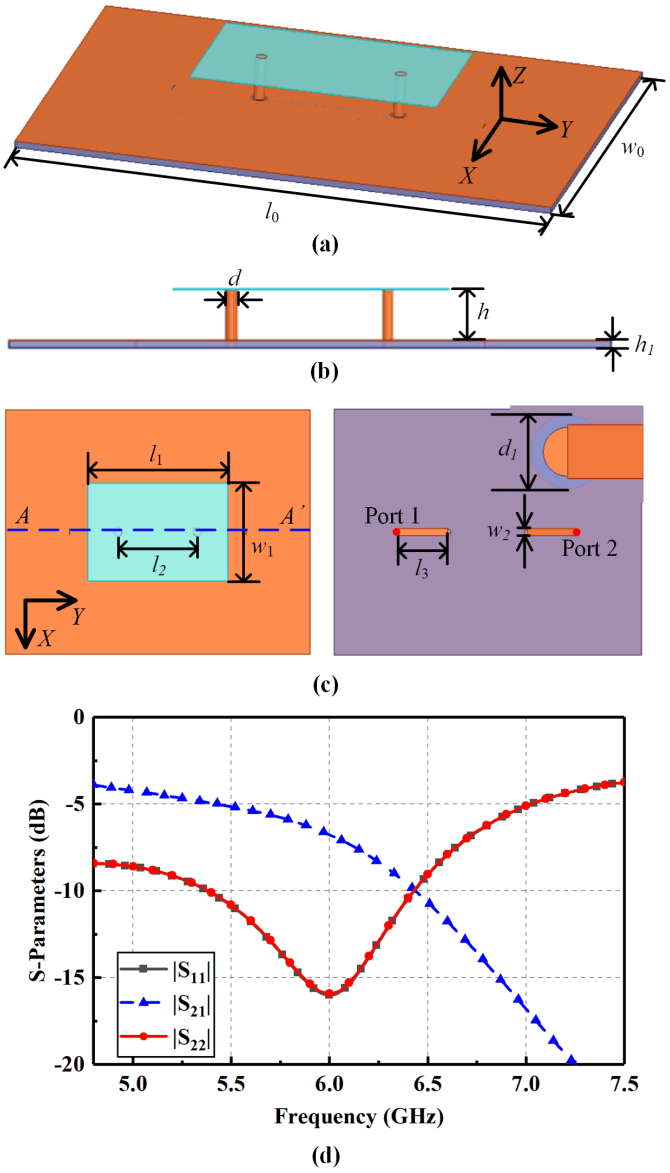

Fig. 4. (a) Perspective, (b) side, and (c) top and bottom views of the two-port MSA I. (d) Simulated S-parameters.

TABLE I
DETAILED DIMENSIONS OF MSA I

Parameter	Value(mm)	Parameter	Value(mm)
l_0	50	w_2	1.1
l_1	23	d	1
l_2	13	d_1	1.5
l_3	8	h	4
w_0	40	h_1	0.6
w_1	16		

The simulated S-parameters of the two-port MSA are shown in Fig. 4(d). The two ports have the same working bands (5.38–6.43 GHz) due to the symmetrical feature. It can be observed that the mutual coupling level between the two ports is higher than −10 dB around 6 GHz. Therefore, broadband decoupling results cannot be obtained by directly loading filters on MSA I.

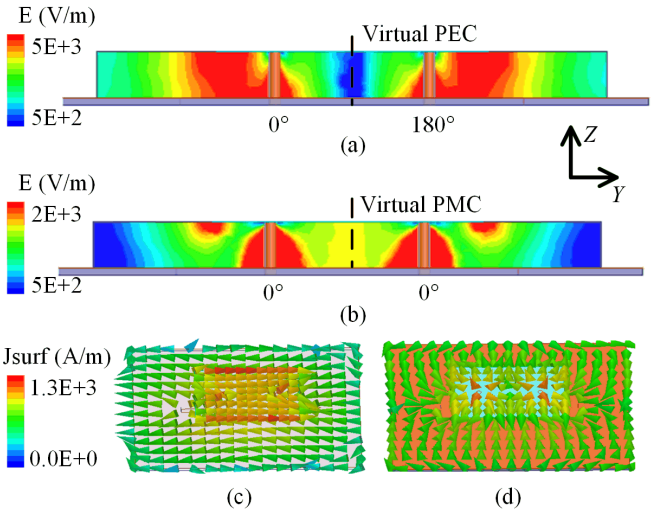

Fig. 5. Simulated electric field intensity distributions of (a) DM and (b) CM of MSA I at 6 GHz. The current distributions of (c) DM and (d) CM.

The CM/DM cancellation theory has been proposed in [24] and offers a new decoupling perspective. Based on the decoupling method, many works realized port decoupling in the same frequency bands [8], [24], [25]. In-phase input and out-of-phase input are used to obtain CM and DM status, respectively. In a symmetrical, reciprocal two-port network described by S-parameters (S_{ij}), the mutual coupling can be expressed by the reflection coefficient of CM (S_{cc11}) and DM (S_{dd11}) [24]

$$S_{21} = S_{12} = \frac{S_{cc11} - S_{dd11}}{2}. \tag{1}$$

To realize ideal isolation, the equation $S_{cc11} = S_{dd11}$ should be satisfied. Hence, a feasible way is needed to independently tune the S_{cc11} and S_{dd11} status for realizing high isolation.

As shown in Fig. 5, when the two ports of MSA I are fed with in-phase and out-of-phase signals, weak and strong electric field intensity distributions are obtained in the center plane (yz plane). Hence, the center plane can be equivalent to virtual PEC and virtual PMC planes under DM and CM status, respectively. Fig. 5(c) and (d) shows the current distributions of DM and CM, respectively. The two current distributions show a significant difference. Then, an effective way is needed to tune CM and DM impedances to the same status for achieving high isolation.

Fig. 6(a) and (b) shows the perspective and bottom views of MSA II. In order to realize port decoupling, a probe is utilized to load in the central plane. An equivalent capacitance C can be obtained between the decoupling probe and the ground, as shown in Fig. 6(a). The equivalent capacitance values can be adjusted by changing the parameter d_3. As shown in Fig. 6(b), two lumped inductors L_1 and L_2 were utilized to realize port matching. The two ports operate near 6 GHz with $L_1 = L_2 = 1.5$ nH.

Fig. 6(c) shows the influence of the equivalent capacitance C on CM and DM impedance by changing the parameter d_3. As shown in Fig. 6(c), the equivalent capacitance only adjusts the CM impedance due to the virtual PMC boundary

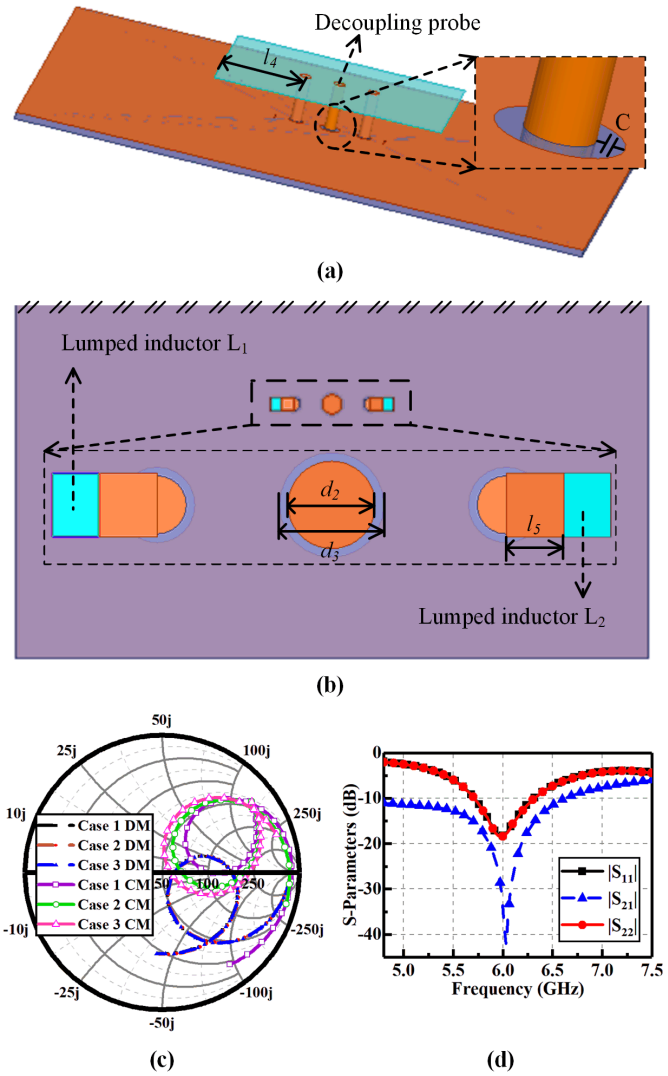

Fig. 6. (a) Perspective and (b) bottom views of MSA II. (c) Smith chart of DM and CM impedances corresponding to different cases. Case 1: $d_3 = 0.2$ mm. Case 2: $d_3 = 0.4$ mm. Case 3: $d_3 = 0.6$ mm. (d) Simulated S-parameters. Detailed dimensions: $l_4 = 7$ mm, $l_4 = 1$ mm, $d_2 = 1.5$ mm, and $d_3 = 1.8$ mm.

of CM. To achieve port decoupling at 6 GHz, $d_3 = 0.4$ mm is selected finally. Fig. 6(d) shows the simulated S-parameters of MSA II. The simulated operating bandwidth for the two ports is 5.71–6.31 GHz with a maximum isolation value of 42 dB at 6.03 GHz. According to the above analysis, the orthogonal modes of antenna (CM and DM) are used to characterize the decoupling level and guide the decoupling process, rather than being excited [21], [22]. In this article, the port-to-port decoupling is achieved by loading a simple probe without complex decoupling networks.

B. Port Matching

In Section II-A, port decoupling is realized by loading a decoupling probe with $|S_{11}| = |S_{22}|$. To simultaneously support Wi-Fi 6 and Wi-Fi 6E standards, the operating frequencies of one port should be moved to lower frequencies, while that of the other port should be tuned to higher frequencies. Moreover, it is undesirable that $|S_{21}|$ changes with the variation of $|S_{11}|$ and $|S_{22}|$.

The reflection coefficient of CM (S_{cc11}) and DM (S_{dd11}) can be expressed by the S-parameters (S_{ij})

$$S_{cc11} = \frac{S_{11} + S_{21} + S_{12} + S_{22}}{2}$$
$$S_{dd11} = \frac{S_{11} - S_{21} - S_{12} + S_{22}}{2}. \quad (2)$$

Specifically, a reciprocal two-port network satisfies the condition of $S_{12} = S_{21}$. S_{12} and S_{21} are ignorable if the mutual coupling is effectively reduced with $|S_{11}|$ and $|S_{22}|$ less than -10 dB at frequency f_0. Hence, the formulas of S_{cc11} and S_{dd11} at f_0 can be simplified to

$$S_{cc11} \approx \frac{S_{11} + S_{22}}{2}$$
$$S_{dd11} \approx \frac{S_{11} + S_{22}}{2}. \quad (3)$$

According to (3), we can conclude that the equation $S_{cc11} \approx S_{dd11}$ is always true at f_0 even if S_{11} and S_{22} change, that is to say, for a reciprocal two-port antenna system, if the CM and DM impedances are the same at f_0, the operating frequencies of two ports can be independently tuned but without deteriorating the isolation at f_0.

Accordingly, the working frequencies of two ports can be tuned to different frequency bands by using distinct matching circuits. As shown in Fig. 7(a), matching circuits based on microstrip and lumped inductors are applied with other antenna parameters unchanged. As shown in Fig. 7(b), the simulated -10 dB bandwidth of Ports 1 and 2 is 5.41–6.07 and 5.58–7.49 GHz, respectively, with high isolation near 6 GHz. To further prove this point, the effects of the different matching statuses of two ports on the mutual coupling were studied. Fig. 8(a) and (b) shows the variation of S-parameters with different values of L_1 and L_2, respectively. High isolation around 6 GHz is maintained with various values of L_1 and L_2. This phenomenon demonstrates that different matching status of the two ports has a limited impact on the original isolation.

Based on the analysis above, there are three steps to realize broadband decoupling for the strongly coupled two-port MSA antennas.

Step 1: Based on the concerned frequency of the two ports with adjacent/continuous operating bands, the original size of antenna is determined. By loading a decoupling probe, the CM impedance is independently tuned and close to its DM impedance at the concerned frequency. The two ports are well-matched at the target frequency by using lumped inductors. Hence, high isolation and port matching are realized at the concerned frequency.

Step 2: By applying different matching circuits, the operating frequencies of the two ports can be adjusted independently without deteriorating the original isolation. Therefore, the two ports can support different communication standards.

Step 3: By adding preselected filters, broadband decoupling is achieved.

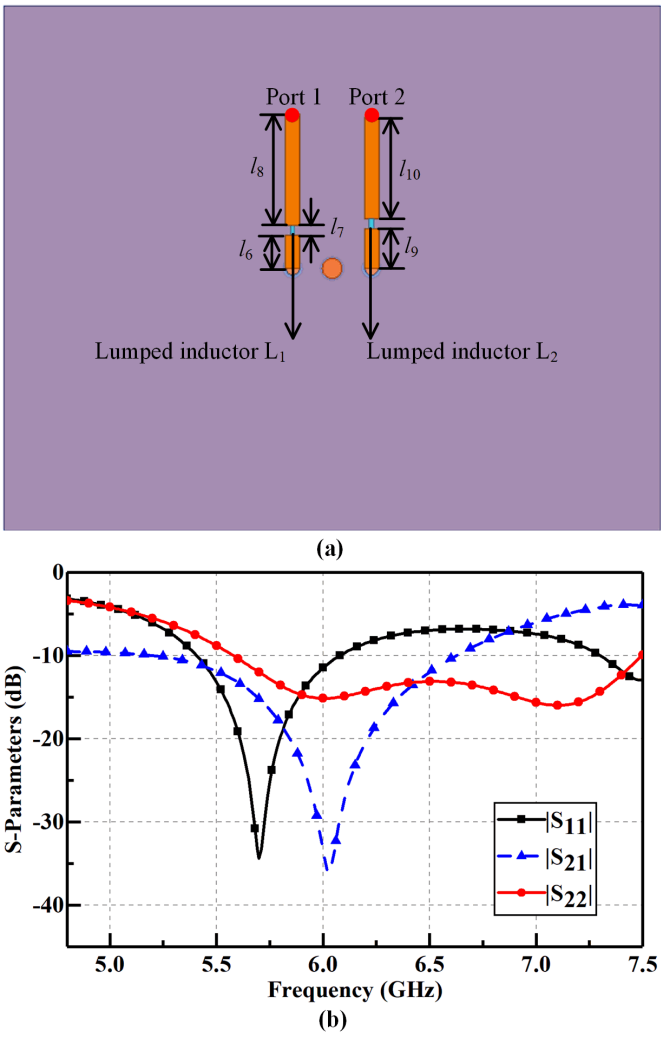

Fig. 7. (a) Bottom view of the MSA III. (b) Simulated S-parameters. Detailed dimensions: $l_6 = 2.5$ mm, $l_7 = 0.8$ mm, $l_8 = 8.5$ mm, $l_9 = 3$ mm, $l_{10} = 7.7$ mm, $L_1 = 1.5$ nH, and $L_2 = 0.7$ nH.

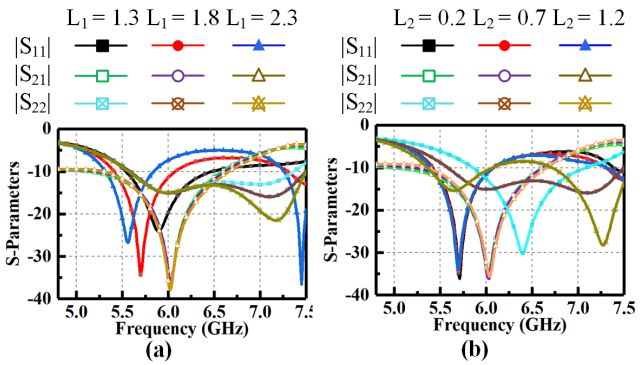

Fig. 8. S-parameters for different values of (a) L_1 and (b) L_2 (unit: nH).

III. Experimental Verification

To validate the proposed antenna, a prototype was fabricated and measured. Fig. 9(a) and (b) shows the top and bottom views of the prototype. The antenna's feeding network is composed of two lumped inductors and two filters (Johanson 5697CR45A0360 and Johanson 6530BP44A1190). The metal was manufactured by 0.3 mm-thick brass plates

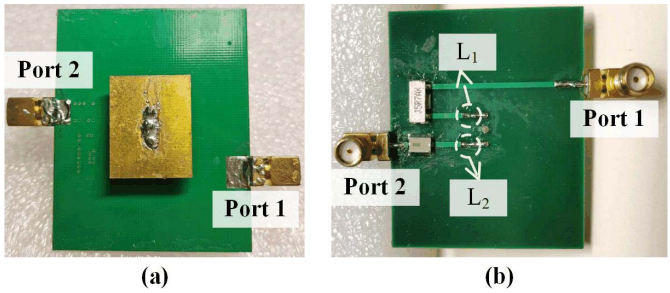

Fig. 9. Fabricated prototype of the proposed antenna. (a) Front and (b) bottom views.

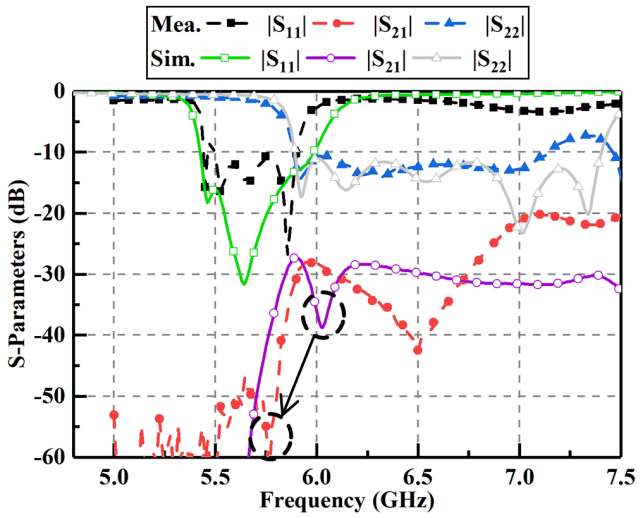

Fig. 10. Simulated and measured S-parameters of the proposed antenna.

($\sigma = 1.5 \times 10^7$ S/m) with a laser cutting process. Two SMAs were used to feed the antenna with inner conductors soldered on the microstrip line and outer conductors connected with the ground. The characteristic impedances of the two transmission lines connecting port and filter are 50 Ω. The S-parameters of the antenna were measured by a vector network analyzer (Agilent N9917A).

Fig. 10 shows the measured and simulated S-parameters of the proposed antenna. The simulated results were obtained based on ADS software. The measured data in general agree well with the simulated results. The measured isolation is higher than 20 dB across the whole operating bandwidth. The simulated operating bands ($|S_{11}| < -10$ dB) for Ports 1 and 2 are 5.43–5.98 and 5.90–7.40 GHz, respectively, while the measured ones for Ports 1 and 2 are 5.49–5.90 and 5.89–7.14 GHz, respectively. Compared with the simulated results, the dip of measured isolation moves to a lower frequency. These discrepancies between the measurement and the simulation are mainly caused by the fabrication soldering error and the tolerance of lumped components. One important parameter was studied, namely, the profile (h) of the MSA III. Fig. 11 shows the simulated S-parameters with different values of h. The increase of parameter h contributes to the reduction of the working frequencies of $|S_{11}|$ and $|S_{21}|$. Besides, the change of h has a great effect on the matching status of Port 2 at higher frequency band. Therefore, the discrepancy

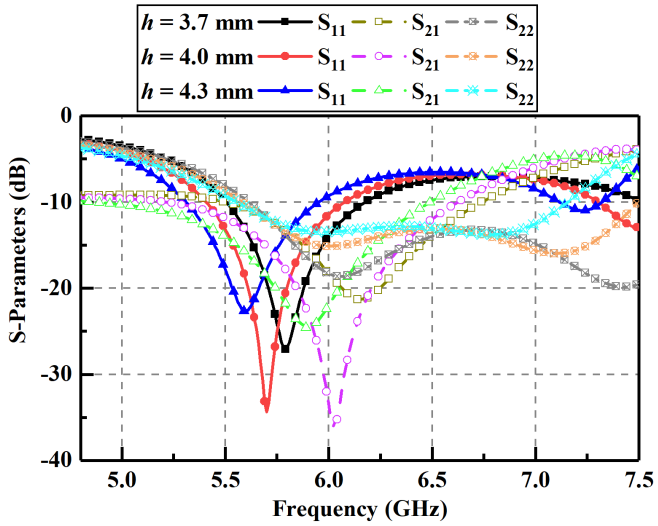

Fig. 11. *S*-parameters for different profiles of MSA III.

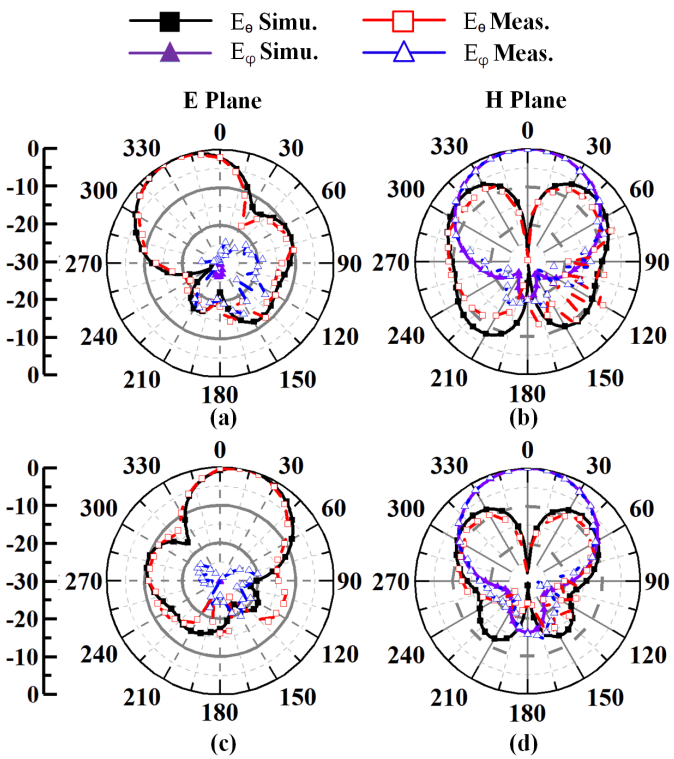

Fig. 12. Simulated and measured normalized radiation patterns of the proposed antenna. Port 1 in (a) *yz* plane and (b) *xz* plane at 5.7 GHz. Port 2 in (c) *yz* plane and (d) *xz* plane at 6.5 GHz.

between the measured and simulated results is mainly caused by the soldering error.

The simulated and measured normalized radiation patterns of the fabricated prototypes are shown in Fig. 12. The radiation patterns were measured in a far-field anechoic chamber. It can be seen that the measured results have a good agreement with the simulations. Opposite tilted beams are observed for the two ports in the *yz* plane. This phenomenon can be explained from the perspective of the CM and DM. The relationship of radiation patterns for MSA III at 6 GHz is shown in Fig. 13. In the case DM 1, the feed phases of Ports 1 and 2 are 0°and

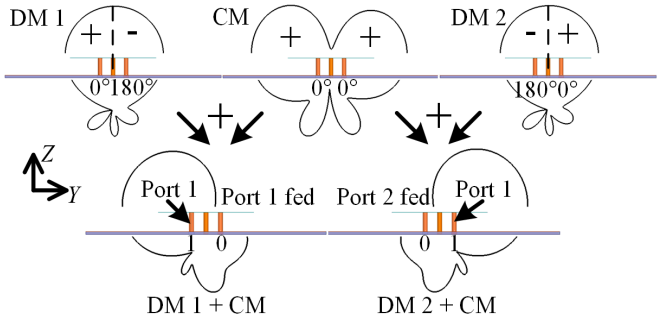

Fig. 13. Schematic of the radiation patterns for each port from the perspective of the CM and DM.

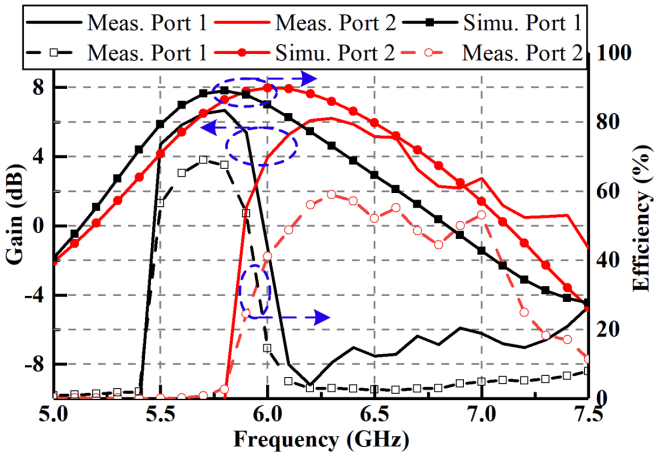

Fig. 14. Measured gains and efficiency of the proposed antenna.

180°, respectively, while in the case DM 2, the two feed phases are reversed. Broadside and omnidirectional patterns are obtained in DM 1/2 and CM, respectively. The plus and minus signs represent the relative phase relation between the two ports. The radiation pattern of Port 1 can be obtained by superposing the CM and DM 1. The radiation pattern tilts to the left with Port 1 excited and Port 2 loaded with 50 Ω due to the phase difference. Similarly, the right tilted beam is obtained when Port 2 is excited.

The measured peak gains and efficiency of two ports are shown in Fig. 14. In addition, the simulated efficiency of the MSA III is also given for comparison. For MSA III, high simulated efficiency for the two ports is obtained around 6 GHz. With the frequency moving away from 6 GHz, the mutual coupling between the two ports of MSA III increases, which decreases the efficiency of the two ports. The measured gains and efficiency of two ports are lower than traditional MSAs mainly due to the insertion loss of the two filters. The typical insertion loss of the Johanson 5697CR45A0360 and Johanson 6530BP44A1190 filters is 1.7 and 2.3 dB, respectively. In future studies, a wideband decoupling method for antenna systems with adjacent/continuous working bands is desired. As seen, the peak gains are relatively low near 7 GHz. This phenomenon can be explained that the performance of the antenna at higher operating frequencies is sensitive to the soldering error, as shown in Fig. 11.

A comprehensive comparison between the proposed antenna and other relevant studies is given in Table II. As seen,

TABLE II
PERFORMANCES COMPARISON WITH RELEVANT STUDIES

Ref.	Method	Frequency (GHz)	Original Isolation (dB)	Isolation (dB)	Edge to edge spacing (λ_0)
[12]	Filtering structures	4.45 - 5.10/ 5.20 - 5.40	14	23	0.02
[13]	Band-notched slot antenna	1.65-1.88/ 1.89-2.22	17	25	0.29
[17]	Filtering structures	1.62-1.88/ 1.92-2.30	22	31	0.30
[18]	Decoupling network & Filters	2.29-2.41/ 2.40-2.50	25	45	3.04
[20]	Decoupling network	2.30-2.40/ 2.40-2.48	20	41	0.59
Pro.	CM/DM cancellation & Filters	5.49 – 5.90/ 5.89 - 7.14	6.7	20	0

Original Isolation: the minimum isolation at the concerned frequency band of two ports with close/continuous working frequencies. Isolation: the measured minimum isolation over the whole operating bandwidth. λ_0: the free-space wavelength at the center frequency.

the minimum original isolation at common edge frequencies among the published works is higher than 14 dB. In this work, though the two ports have the smallest original isolation and continuous operating bands, high isolation is realized across the whole working bandwidth. Compared to other works, the smallest edge-to-edge spacing is obtained in this work.

IV. CONCLUSION

In this work, a compact two-port MSA with high isolation is proposed for simultaneously supporting Wi-Fi 6 and Wi-Fi 6E applications. The proposed antenna is designed based on the CM/DM cancellation theory and filters. The design guideline is given in detail. Such a design has the potential to play an important role in future communication systems that support Wi-Fi 6 and Wi-Fi 6E standards simultaneously. Also, the decoupling process could be applied to other antenna systems with close/continuous operating frequencies.

REFERENCES

[1] Z. Hu, Z. Chen, R. Susitaival, I.-F. Fu, S. K. Baghel, and P. Dayal, "Interference avoidance for in-device coexistence in 3 GPP LTE-advanced: Challenges and solutions," *IEEE Commun. Mag.*, vol. 50, no. 11, pp. 60–67, Nov. 2012.

[2] W. Zhang, J. Hu, Y. Li, and Z. Zhang, "Design of a stacked co-polarized full-duplex antenna with broadside radiation," *IEEE Trans. Antennas Propag.*, vol. 69, no. 11, pp. 7111–7118, Nov. 2021.

[3] L. Sun, Y. Li, Z. Zhang, and Z. Feng, "Compact co-horizontally polarized full-duplex antenna with omnidirectional patterns," *IEEE Antennas Wireless Propag. Lett.*, vol. 18, no. 6, pp. 1154–1158, Jun. 2019.

[4] K. Iwamoto, M. Heino, K. Haneda, and H. Morikawa, "Design of an antenna decoupling structure for an inband full-duplex collinear dipole array," *IEEE Trans. Antennas Propag.*, vol. 66, no. 7, pp. 3763–3768, Jul. 2018.

[5] Y. He and Y. Li, "Compact co-linearly polarized microstrip antenna with fence-strip resonator loading for in-band full-duplex systems," *IEEE Trans. Antennas Propag.*, vol. 69, no. 11, pp. 7125–7133, Nov. 2021.

[6] S. Manafi, M. A. Al-Tarifi, and D. S. Filipovic, "Isolation improvement techniques for wideband millimeter-wave repeaters," *IEEE Antennas Wireless Propag. Lett.*, vol. 17, no. 2, pp. 355–358, Feb. 2018.

[7] Z. Zhou, Y. Li, J. Hu, Y. He, Z. Zhang, and P.-Y. Chen, "Monostatic copolarized simultaneous transmit and receive (STAR) antenna by integrated single-layer design," *IEEE Antennas Wireless Propag. Lett.*, vol. 18, no. 3, pp. 472–476, Mar. 2019.

[8] J. Hu, W. Zhang, Y. Li, and Z. Zhang, "Compact co-polarized PIFAs for full-duplex application based on CM/DM cancellation theory," *IEEE Trans. Antennas Propag.*, vol. 69, no. 11, pp. 7103–7110, Nov. 2021.

[9] Y. Cui, R. Li, and P. Wang, "Novel dual-broadband planar antenna and its array for 2G/3G/LTE base stations," *IEEE Trans. Antennas Propag.*, vol. 61, no. 3, pp. 1132–1139, Mar. 2013.

[10] L. Y. Nie *et al.*, "A low-profile coplanar dual-polarized and dual-band base station antenna array," *IEEE Trans. Antennas Propag.*, vol. 66, no. 12, pp. 6921–6929, Dec. 2018.

[11] H.-H. Sun, C. Ding, H. Zhu, B. Jones, and Y. J. Guo, "Suppression of cross-band scattering in multiband antenna arrays," *IEEE Trans. Antennas Propag.*, vol. 67, no. 4, pp. 2379–2389, Apr. 2019.

[12] J. Guo, F. Liu, L. Zhao, G.-L. Huang, Y. Li, and Y. Yin, "Isolation improvement of two tightly coupled antennas operating in adjacent frequency bands using filtering structures," *IEEE Open J. Antennas Propag.*, vol. 1, pp. 207–214, 2020.

[13] M. Li, R. Wang, J. M. Yasir, and L. Jiang, "A miniaturized dual-band dual-polarized band-notched slot antenna array with high isolation for base station applications," *IEEE Trans. Antennas Propag.*, vol. 68, no. 2, pp. 795–804, Feb. 2020.

[14] L. Zhao, F. Liu, X. Shen, G. Jing, Y.-M. Cai, and Y. Li, "A high-pass antenna interference cancellation chip for mutual coupling reduction of antennas in contiguous frequency bands," *IEEE Access*, vol. 6, pp. 38097–38105, 2018.

[15] B. C. Pan and K. J. Cui, "Broadband decoupling network for dual-band microstrip patch antennas," *IEEE Trans. Antennas Propag.*, vol. 65, no. 10, pp. 5595–5598, Oct. 2017.

[16] M. Li, Q. Li, B. Wang, C. Zhou, and S. Cheung, "A miniaturized dual-band base station array antenna using band notch dipole antenna elements and AMC reflectors," *IEEE Trans. Antennas Propag.*, vol. 66, no. 6, pp. 3189–3194, Jun. 2018.

[17] Y. Zhang, X. Y. Zhang, L.-H. Ye, and Y.-M. Pan, "Dual-band base station array using filtering antenna elements for mutual coupling suppression," *IEEE Trans. Antennas Propag.*, vol. 64, no. 8, pp. 3423–3430, Aug. 2016.

[18] L. Zhao, K.-W. Qian, and K.-L. Wu, "A cascaded coupled resonator decoupling network for mitigating interference between two radios in adjacent frequency bands," *IEEE Trans. Microw. Theory Techn.*, vol. 62, no. 11, pp. 2680–2688, Nov. 2014.

[19] K.-W. Qian, "A compact LTCC decoupling-network based on coupled-resonator for antenna interference suppression of adjacent frequency bands," *IEEE Access*, vol. 7, pp. 25485–25492, 2019.

[20] M. Li, M. Wang, L. Jiang, and L. K. Yeung, "Decoupling of antennas with adjacent frequency bands using cascaded decoupling network," *IEEE Trans. Antennas Propag.*, vol. 69, no. 2, pp. 1173–1178, Feb. 2021.

[21] C. Volmer, J. Weber, R. Stephan, K. Blau, and M. A. Hein, "An eigen-analysis of compact antenna arrays and its application to port decoupling," *IEEE Trans. Antennas Propag.*, vol. 56, no. 2, pp. 360–370, Feb. 2008.

[22] L. K. Yeung and Y. E. Wang, "Mode-based beamforming arrays for miniaturized platforms," *IEEE Trans. Microw. Theory Techn.*, vol. 57, no. 1, pp. 45–52, Jan. 2009.

[23] X. Guan, F. Yang, H. Liu, and L. Zhu, "Compact and high-isolation diplexer using dual-mode stub-loaded resonators," *IEEE Microw. Wireless Compon. Lett.*, vol. 24, no. 6, pp. 385–387, Jun. 2014.

[24] L. Sun, Y. Li, Z. Zhang, and H. Wang, "Antenna decoupling by common and differential modes cancellation," *IEEE Trans. Antennas Propag.*, vol. 69, no. 2, pp. 672–682, Feb. 2021.

[25] L. Sun, Y. Li, and Z. Zhang, "Decoupling between extremely closely spaced patch antennas by mode cancellation method," *IEEE Trans. Antennas Propag.*, vol. 69, no. 6, pp. 3074–3083, Jun. 2021.

[26] Ansoft Corp., Pittsburgh, PA, USA. *HFSS V15*. Accessed: Aug. 10, 2021. [Online]. Available: http://www.ansys.com/products/electronics/ansyshfss

Weiquan Zhang received the B.S. degree from the University of Electronic Science and Technology of China, Chengdu, China, in 2018. He is currently pursuing the Ph.D. degree in electrical engineering with Tsinghua University, Beijing, China.

His current research interests include reconfigurable antennas, multimode antennas, and reflectarray antennas.

Yue Li (Senior Member, IEEE) received the B.S. degree in telecommunication engineering from Zhejiang University, Zhejiang, China, in 2007, and the Ph.D. degree in electronic engineering from Tsinghua University, Beijing, China, in 2012.

In June 2012, he was a Post-Doctoral Fellow with the Department of Electronic Engineering, Tsinghua University, where he is currently an Associate Professor. In December 2013, he was a Research Scholar with the Department of Electrical and Systems Engineering, University of Pennsylvania, Philadelphia, PA, USA. He was a Visiting Scholar with the Institute for Infocomm Research (I2R), A∗STAR, Singapore, in 2010, and the Hawaii Center of Advanced Communication (HCAC), University of Hawaii, Manoa, Honolulu, HI, USA, in 2012. Since January 2016, he has been with Tsinghua University, where he is currently an Assistant Professor. He has authored and coauthored over 170 journal articles and 50 international conference papers. He holds 25 granted Chinese patents. His current research interests include metamaterials, plasmonics, electromagnetics, nanocircuits, mobile and handset antennas, MIMO and diversity antennas, and millimeter-wave antennas and arrays.

Dr. Li was a recipient of the Issac Koga Gold Medal from URSI General Assembly in 2017; the Second Prize of Science and Technology Award of China Institute of Communications in 2017; and the Young Scientist Awards from the conferences of PIERS 2019, ACES 2018, AT-RASC 2018, AP-RASC 2016, EMTS 2016, and URSI GASS 2014. He is serving as an Associate Editor for IEEE TRANSACTIONS ON ANTENNAS AND PROPAGATION, IEEE ANTENNAS AND WIRELESS PROPAGATION LETTERS, *Microwave and Optical Technology Letters*, and *Computer Applications in Engineering Education*. He is serving on the Editorial Board of *Scientific Report*, *Sensors* (MDPI), and *Electronics* (MDPI).

Kunpeng Wei (Senior Member, IEEE) received the B.S. degree in electronic and information engineering from the Huazhong University of Science and Technology, Wuhan, China, in 2008, and the Ph.D. degree in electrical engineering from Tsinghua University, Beijing, China, in 2013.

From July 2013 to December 2015, he was employed at the Radar Research Institute, Chinese Air Force Research Laboratory, Beijing, conducting research in the areas of phased-array antenna design and radar system design. He joined the Consume Business Group, Huawei Inc., in 2016, where he had been an Antenna Specialist and the Director of the Xi'an Antenna Team for five years. In 2021, he joined Honor Device Company Ltd., Beijing, China, when this company split from Huawei, where he is currently the Director of the Honor Antenna Team. He leads a large group of antenna engineers and takes the full leadership and responsibility in the research and development of antenna technologies to guarantee the market success of all Honor's mobile terminal products ranging from smartphones, laptops, tablets, smartwatches, routers, smart screens, and TWS earphones. He has authored over refereed 50 articles on consumer electronics antenna design. He holds over 15 granted U.S./EU/JP/CN patents and has other more than 30 patent applications in pending. His current research interests include smartphone antenna design, small-size 5G antenna systems in terminal devices, and millimeter-wave antenna arrays.

Dr. Wei was a recipient of the Principal Scholarship of Tsinghua University in 2012, the Huawei Individual Gold Medal Award in 2018, the Huawei Team Gold Medal Award in 2017, and the Honor Team Gold Medal Award in 2021. He has been serving as an Associate Editor for *IET Electronics Letters* since October 2021.

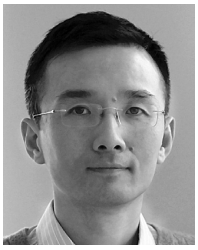

Zhijun Zhang (Fellow, IEEE) received the B.S. and M.S. degrees from the University of Electronic Science and Technology of China, Chengdu, China, in 1992 and 1995, respectively, and the Ph.D. degree from Tsinghua University, Beijing, China, in 1999.

In 1999, he was a Post-Doctoral Fellow with the Department of Electrical Engineering, University of Utah, Salt Lake City, UT, USA, where he was appointed as a Research Assistant Professor in 2001. In May 2002, he was an Assistant Researcher with the University of Hawaii at Manoa, Honolulu, HI, USA. In November 2002, he joined Amphenol T&M Antennas, Vernon Hills, IL, USA, as a Senior Staff Antenna Development Engineer and was then promoted to the position of Antenna Engineer Manager. In 2004, he joined Nokia Inc., San Diego, CA, USA, as a Senior Antenna Design Engineer. In 2006, he joined Apple Inc., Cupertino, CA, USA, as a Senior Antenna Design Engineer and was then promoted to the position of Principal Antenna Engineer. Since August 2007, he has been with Tsinghua University, where he is currently a Professor with the Department of Electronic Engineering. He is the author of *Antenna Design for Mobile Devices* (Wiley, First Edition 2011 and Second Edition 2017).

Dr. Zhang served as an Associate Editor for the IEEE TRANSACTIONS ON ANTENNAS AND PROPAGATION from 2010 to 2014 and the IEEE ANTENNAS AND WIRELESS PROPAGATION LETTERS from 2009 to 2015.